

Research article

Hao Jia^a, Ting Zhou^a, Xin Fu, Jianfeng Ding, Lei Zhang and Lin Yang^{*}

Integrated five-port non-blocking optical router based on mode-selective property

<https://doi.org/10.1515/nanoph-2018-0010>

Received January 25, 2018; revised February 8, 2018; accepted February 10, 2018

Abstract: In this paper, we propose and demonstrate a five-port optical router based on mode-selective property. It utilizes different combinations of four spatial modes at input and output ports as labels to distinguish its 20 routing paths. It can direct signals from the source port to the destination port intelligently without power consumption and additional switching time to realize various path steering. The proposed architecture is constructed by asymmetric directional coupler based mode-multiplexers/de-multiplexers, multimode interference based waveguide crossings and single-mode interconnect waveguides. The broad optical bandwidths of these constituents make the device suitable to combine with wavelength division multiplexing signal transmission, which can effectively increase the data throughput. Measurement results show that the insertion loss of its 20 routing paths are lower than 8.5 dB and the optical signal-to-noise ratios are larger than 16.3 dB at 1525–1565 nm. To characterize its routing functionality, a 40-Gbps data transmission with bit-error-rate (BER) measurement is implemented. The power penalties for the error-free switching ($\text{BER} < 10^{-9}$) are 1.0 dB and 0.8 dB at 1545 nm and 1565 nm, respectively.

Keywords: optical interconnect; silicon photonics; mode-division multiplexing; optical switching.

^a**Hao Jia and Ting Zhou:** These authors contributed equally to this work.

***Corresponding author: Lin Yang**, State Key Laboratory of Integrated Optoelectronics, Institute of Semiconductors, Chinese Academy of Sciences, P. O. Box 912, Beijing 100083, China, e-mail: oip@semi.ac.cn. <http://orcid.org/0000-0003-0671-6459>; and College of Materials Science and Opto-Electronic Technology, University of Chinese Academy of Sciences, Beijing, China

Hao Jia, Ting Zhou, Xin Fu, Jianfeng Ding and Lei Zhang: State Key Laboratory of Integrated Optoelectronics, Institute of Semiconductors, Chinese Academy of Sciences, P. O. Box 912, Beijing 100083, China; and College of Materials Science and Opto-Electronic Technology, University of Chinese Academy of Sciences, Beijing, China

1 Introduction

Optical interconnect offers a communication backbone that has the highest level of capacity and reliability [1, 2]. Photonics network-on-chip (NoC), which capitalizes on the benefits of optical interconnect, such as large capacity, low latency and low power consumption, has been proposed as a promising alternative to traditional metallic interconnect for large-scale multiple processor cores [3, 4]. As the key component of NoC, the optical router undertakes the function of routing signals from input ports to desired output ports.

Lots of optical routers and switches have been reported [5–19]. Among them, the four-port and five-port optical routers have received wide attention as they are commonly used as building blocks of many photonic NoC architectures [5–13]. Compared with optical routers with dynamically established routing paths, optical routers with passively established routing paths are much more energy-efficient and have no switching time on the expense of fixed routing paths [8–10, 15, 18]. Wavelength-selective optical router is a stereotype, which utilizes the freedom of wavelength, although the wavelength-selective characteristic intrinsically limits its optical bandwidth. Moreover, the resonance components that have been used to realize wavelength selectivity are sensitive to environmental temperature variation. Recently mode division multiplexing (MDM) offers a new dimension to scale on-chip optical interconnect by utilizing the spatial modes of waveguides to carry multiple optical signals simultaneously. Correspondingly, many devices for MDM such as mode multiplexers/de-multiplexers, multimode waveguide crossings and multimode waveguide bends have been reported [20–27]. Similar to wavelength selectivity, mode selectivity utilizes different spatial modes and can also be considered as a new degree of freedom to construct optical routers. Combining MDM technologies with optical router can offer new potentials in high-throughput, high-stability passive data routing.

In this paper, we propose and experimentally demonstrate a five-port optical router using the mode-selective property. It utilizes the different combinations of four

spatial modes at input and output ports as labels to distinguish its 20 routing paths, and it can passively direct signals from the source port to the destination port intelligently without power consumptions and additional switching time to realize various path steering. The multicast capability can be realized by importing MDM signals to each port. The architecture is constructed by five asymmetric directional coupler based mode multiplexers/de-multiplexers, nine multimode interference based waveguide crossings and 10 single-mode interconnect waveguides. These components have broad optical bandwidths, so the constructed device is suitable for wavelength-division multiplexing signal transmission. Experimental results show that the insertion loss of its 20 routing paths are less than 8.5 dB and the optical signal-to-noise ratios (OSNRs) are larger than 16.3 dB in the worst case. To characterize its routing functionality, a 40-Gbps data transmission with bit-error-rate (BER) measurement is implemented at both 1545 nm and 1565 nm.

2 Architecture design and device fabrication

Generally, each routing path of passive routing optical routers is pre-designed and fixed in advance. As signal injected into one port is unnecessary to be back to itself, we combine the corresponding input and output ports into a unique port with bidirectional data transmission to simplify the architecture design and reduce the footprint. The five ports of our proposed device are defined as P_1 , P_2 , P_3 , P_4 and P_5 , respectively. Each port supports both upstream signals and downstream signals. Similar to wavelength-selective routing, signals injected into one port at different spatial modes will be routed to different target ports in mode-selective routing. For example, if signals at four different modes M_1 , M_2 , M_3 and M_4 are injected into P_1 , they can be assigned to P_2 , P_3 , P_4 and P_5 , respectively. To effectively utilize the spatial mode channel resources, we assign

a minimal number of spatial modes in the architecture to fulfill the one-by-one mapping of input-output port pairs and input-output mode combinations so that all routing paths can be distinguished and the communications among them can be established simultaneously without confliction. Specific to our five-port optical router, each port supports multiple spatial modes and needs to be communicated with the other four ports. To avoid blocking among routing paths, at least four spatial modes are required. We select the four lowest-order guided modes TE_0 , TE_1 , TE_2 , and TE_3 in multimode waveguide and assign them suitably to fulfill the non-blocking communication of the whole 20 routing paths of the five-port optical router. The mapping of input-output spatial mode combinations and the routing paths are listed in Table 1. Each item including two modes and an arrow represents the combination of assigned input/output modes for the corresponding routing paths. Signal injected at the mode of arrow left from the input port is sent to the target output port and converted to the mode of arrow right for distinguishing the source port.

The rule of the mode-selective routing can be explained as follows. Selecting a specific port as viewpoint, there are four other ports remaining for communication. To make the explanation convenient, we reorder the sequence of the remaining four ports as first, second, third and fourth based on their original sequence of port number. If the selected port functions as an input port, the signal sent at mode TE_i ($i=0, 1, 2, 3$) is guided to the $(i+1)$ th port. If it functions as an output port, signals received at mode TE_i is sent from the $(i+1)$ th port. We use P_1 as example to further explain the assignment. There are four remaining ports P_2 , P_3 , P_4 and P_5 that should be communicated with. If P_1 works as an input port, signal sent at TE_0 , TE_1 , TE_2 and TE_3 modes are guided to P_2 , P_3 , P_4 and P_5 , respectively. Oppositely, if P_1 is used as an output port, the received signals at TE_0 , TE_1 , TE_2 and TE_3 modes are sent from P_2 , P_3 , P_4 and P_5 , respectively.

By this one-by-one mapping rule, the passive routing device can be established using mode selectivity. The architecture of the five-port router is shown in Figure 1. Five

Table 1: One-by-one mapping of spatial mode combinations and routing paths of the five-port optical router.

| Input port | Output port | | | | |
|------------|-----------------------------|-----------------------------|-----------------------------|-----------------------------|-----------------------------|
| | P_1 | P_2 | P_3 | P_4 | P_5 |
| P_1 | – | $(TE_0) \rightarrow (TE_0)$ | $(TE_1) \rightarrow (TE_0)$ | $(TE_2) \rightarrow (TE_0)$ | $(TE_3) \rightarrow (TE_0)$ |
| P_2 | $(TE_0) \rightarrow (TE_0)$ | – | $(TE_1) \rightarrow (TE_1)$ | $(TE_2) \rightarrow (TE_1)$ | $(TE_3) \rightarrow (TE_1)$ |
| P_3 | $(TE_0) \rightarrow (TE_1)$ | $(TE_1) \rightarrow (TE_1)$ | – | $(TE_2) \rightarrow (TE_2)$ | $(TE_3) \rightarrow (TE_2)$ |
| P_4 | $(TE_0) \rightarrow (TE_2)$ | $(TE_1) \rightarrow (TE_2)$ | $(TE_2) \rightarrow (TE_2)$ | – | $(TE_3) \rightarrow (TE_2)$ |
| P_5 | $(TE_0) \rightarrow (TE_3)$ | $(TE_1) \rightarrow (TE_3)$ | $(TE_2) \rightarrow (TE_3)$ | $(TE_3) \rightarrow (TE_3)$ | – |

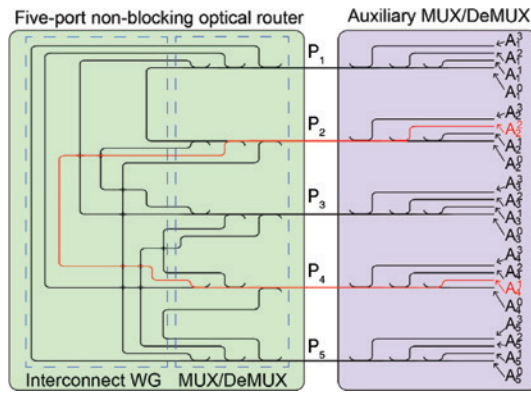


Figure 1: Architecture of the five-port optical router based on mode-selective property (MUX, multiplexer; DeMUX, de-multiplexer; WG, waveguide).

four-channel mode multiplexers/de-multiplexers are connected behind ports P_i . Their function is to multiplex fundamental mode signals and convert them to suitable mode orders in P_i or to de-multiplex the multiplexed signals into fundamental mode ones and assign them to different single-mode waveguides by the original mode order. The implemented function is decided by the signal flow direction. We select asymmetric directional coupler (ADC) as a unit to construct the mode multiplexer/de-multiplexer as it is compact, easy to scale and has relative large optical bandwidth [24]. Ten single-mode interconnect waveguides are used to connect the single-mode waveguide of each ADC by the rule of Table 1 to realize the one-by-one mapping of the routing path. Considering the device characterization, optical fibers should be introduced for input and output. While the coupling between multimode fiber and multimode waveguide is a challenge work, five auxiliary on-chip mode multiplexers/de-multiplexers are connected before five ports P_1 to P_5 , as shown in the right part of Figure 1. Twenty auxiliary input/output ports are labeled from A_1^0 to A_5^3 . Mark A_i^j ($i=1, 2, 3, 4, 5; j=0, 1, 2, 3$) represents that signal flowing from this auxiliary port is connected to the TE_j mode at port P_i . To better illustrate the characterization process of optical router in next part, the description of the routing paths are substituted by using mark A_i^j . For example, communication of routing path $A_2^2 \rightarrow A_1^1$ is equivalent to that of $P_2(TE_2) \rightarrow P_1(TE_1)$ in the optical router. The related physical connection for this routing path is given as the red line in Figure 1.

The device is fabricated on an 8-inch silicon-on-insulator wafer with a 220-nm-thick top silicon layer and a 3- μm -thick buried silicon dioxide layer at the Institute of Microelectronics, Singapore. A 248-nm deep ultraviolet photolithography is used to define the patterns, and inductively coupled plasma etching is employed to form the

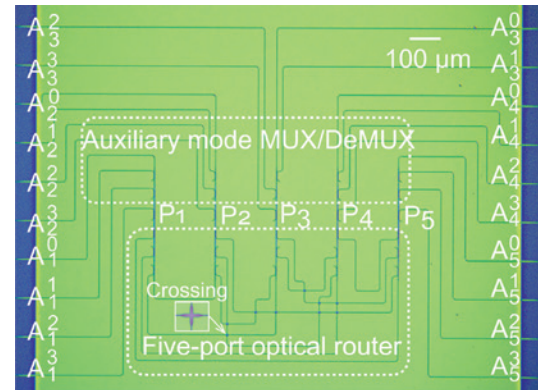


Figure 2: Micrograph of the device.

silicon waveguides. Single-mode rib waveguide is 400 nm in width, 220 nm in height and 70 nm in slab thickness, which only supports the fundamental quasi-TE mode. The widths of the rib waveguides carrying the TE_1 , TE_2 and TE_3 modes are chosen to be 920 nm, 1420 nm and 1920 nm, respectively. A 1500-nm-thick silica layer is deposited on the silicon layer by plasma-enhanced chemical vapor deposition as the cladding layer. Figure 2 shows the micrograph of the fabricated device. Multimode interference based waveguide crossings are used to minimize the propagation loss [28]. A silicon inverse taper covered by an air-bridge silicon dioxide intermediate transition waveguide is used to reduce the coupling loss between the silicon waveguide and the normal single-mode fiber [29, 30].

3 Experimental characterization and discussion

The experimental setup for characterizing the device is shown in Figure 3. Two 10-channel single-mode fiber arrays are utilized to couple light into and out of the device. An amplified spontaneous emission source and an optical spectrum analyzer are utilized to characterize the static spectra of the device. Experimental results show that the coupling loss between waveguide and single-mode fiber is about 3 dB/butt. So a 6-dB coupling loss is deducted for all normalized transmission spectra.

The insertion loss and OSNRs are thoroughly characterized for all 20 routing paths of the router. We take the routing path $A_2^2 \rightarrow A_1^1$ as example to illustrate the method. In this routing path, A_1^1 is served as output port, as shown in Figure 4 (the transmission spectrum of signal is shown in bold red line), and the insertion loss is 2.9–7.8 dB in the wavelength of 1525–1565 nm. Except for the desired signal

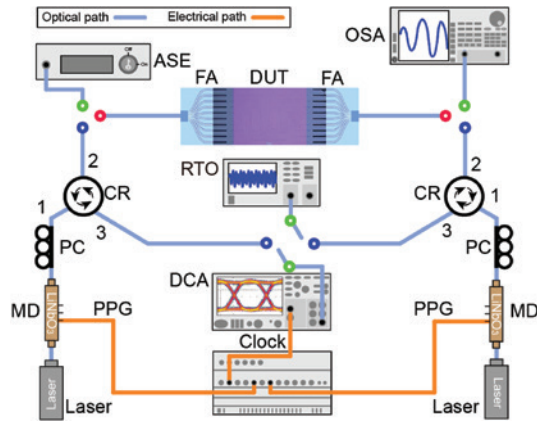


Figure 3: Experimental setup for characterizing the device (ASE, amplified spontaneous emission; TL, tunable laser; PC, polarization controller; DUT, device under test; PPG, pulse pattern generator; OSA, optical spectrum analyzer; DCA, digital communication analyzer; MD, modulator; FA, fiber array; RTO, real-time oscilloscope, CR, circulator).

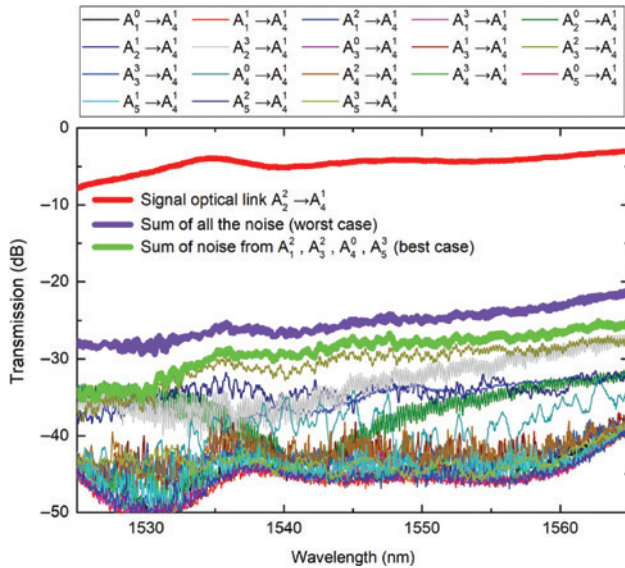


Figure 4: Transmission spectra of signal routing path $A_2^2 \rightarrow A_4^1$ and noise from the other routing paths.

from A_2^2 , signals injected from any other 18 ports may also cause noise to the signal routing path theoretically because of the unexpected leakage; their noise at A_4^1 are measured one by one as shown in normal color lines. In actual application, the light beams are incoherent with each other, so the total noise for one specific routing path is the summation of the noise from individual input. At the worst case, each P_i has four upstream signals and four downstream signals, all auxiliary ports A_i^j have signal input and the total noise is the sum of all noise, which is shown in purple bold lines. The OSNR is 18.1–23.9 dB in the wavelength range from 1525 nm to 1565 nm. In

more common applications, one upstream signal and one downstream signal are occupied for any P_i , which is similar to the routing principle of traditional optical routers. In this case, A_2^2 is used for upstream signal in our example, so A_2^0 , A_2^1 and A_2^3 would not send signal and not cause noise to A_2^2 . Similarly, for the remaining auxiliary input ports, only four inputs could be activated at the same time, each one in charge of loading one upstream signal, and they cause noise to A_2^2 . The total noise is the sum of these four noise. As the conservative estimation, the largest of the four noise is selected. The summation is shown as the green bold line. This case gives the best evaluation of the OSNRs, which is 21.8–29.5 dB.

We calculate the insertion loss and OSNRs of all 20 routing paths; the result is shown in Table 2. Based on the statistics, we can see that in both cases, the insertion loss is lower than 8.5 dB and the OSNRs are larger than 16.3 dB. The main factor leading to the fluctuation of values is the performance variation of ADCs caused by fabrication imperfections. In our device, mode multiplexers for TE_1 and TE_2 modes have relative larger insertion loss and leakage, so the routing paths related to TE_1 mode and TE_2 mode have larger insertion loss and lower OSNRs.

The experimental setup for data transmission is shown in the bottom-half part of Figure 3. As the signal flow through routing paths is bidirectional, two fiber-based three-port circulators are utilized to separate the upstream and downstream signals. The three-port circulator has three ports labeled as 1, 2 and 3. It supports the transmissions of $1 \rightarrow 2$, $2 \rightarrow 3$, and $3 \rightarrow 1$ and blocks the reverse transmissions. Two signal transmitters are used; in each one, a continuous wave light is generated by a tunable laser and injected into a LiNbO_3 optical modulator. A 40-Gbps pseudo-random binary sequence with a length of 2^9-1 is generated by a multi-channel pulse pattern generator and adopted to drive the LiNbO_3 optical modulators. Two modulated optical signals are coupled into and out of the device through the three-port circulator. The signal outputs from on-chip transmission are sent into a digital communication analyzer and a real-time oscilloscope for eye diagram observation and BER measurement, respectively. We also choose the routing path $A_2^2 \rightarrow A_4^1$ for characterization. Figure 5 shows the observed eye diagrams and BERs at 1545 nm and 1565 nm. Compared with the back-to-back signal, eye diagrams after on-chip routing are clear and open, which are not much deteriorated. The power penalties for the error-free switching ($\text{BER} < 10^{-9}$) are 1.0 dB and 0.8 dB at the 1545 nm and 1565 nm, respectively. Based on the standard of International Telecommunication Union, channel spacing of 100 GHz is commonly used, so there are 50 channels in the

Table 2: Statistics of ILs and OSNRs for the five-port optical router (unit/dB).

| | Routing paths | | | | | | |
|-----------------|---------------------------|---------------------------|---------------------------|---------------------------|---------------------------|---------------------------|---------------------------|
| | $A_1^0 \rightarrow A_2^0$ | $A_1^1 \rightarrow A_3^0$ | $A_1^2 \rightarrow A_4^0$ | $A_1^3 \rightarrow A_5^0$ | $A_2^0 \rightarrow A_1^0$ | $A_2^1 \rightarrow A_3^1$ | $A_2^2 \rightarrow A_4^1$ |
| IL | 1.1–4.4 | 1.1–5.3 | 1.0–4.8 | 1.2–4.8 | 1.1–4.4 | 3.2–8.5 | 2.9–7.8 |
| Worst-case OSNR | 22.7–28.5 | 19.2–23.9 | 20.1–23.1 | 19.8–24.9 | 22.3–28.6 | 17.2–21.5 | 18.1–23.9 |
| Best-case OSNR | 26.4–34.5 | 24.4–28.8 | 25.6–32.4 | 25.5–32.4 | 27.3–35.5 | 20.0–26.8 | 21.8–29.5 |
| | $A_3^2 \rightarrow A_1^1$ | $A_3^0 \rightarrow A_1^1$ | $A_3^1 \rightarrow A_2^1$ | $A_3^2 \rightarrow A_4^2$ | $A_3^3 \rightarrow A_5^2$ | $A_4^0 \rightarrow A_1^2$ | $A_4^1 \rightarrow A_2^2$ |
| | | | | | | | |
| IL | 2.8–6.9 | 1.1–5.3 | 3.2–8.5 | 2.2–7.9 | 2.2–6.2 | 1.0–4.8 | 2.9–7.8 |
| Worst-case OSNR | 18.6–24.7 | 22.3–29.3 | 18.9–23.1 | 16.3–19.9 | 17.2–23.1 | 18.5–22.5 | 18.7–23.2 |
| Best-case OSNR | 21.5–28.4 | 27.1–35.4 | 23.4–29.1 | 18.2–24.7 | 18.8–25.9 | 20.9–25.0 | 21.2–25.1 |
| | $A_4^2 \rightarrow A_3^2$ | $A_4^1 \rightarrow A_5^3$ | $A_5^0 \rightarrow A_3^1$ | $A_5^1 \rightarrow A_2^3$ | $A_5^2 \rightarrow A_3^3$ | $A_5^3 \rightarrow A_4^3$ | |
| | | | | | | | |
| IL | 2.2–7.9 | 1.8–6.3 | 1.2–4.8 | 2.8–6.9 | 2.2–6.2 | 1.8–6.3 | – |
| Worst-case OSNR | 16.7–19.5 | 16.6–19.6 | 20.3–22.2 | 19.4–26.4 | 17.2–22.9 | 18.6–24.4 | – |
| Best-case OSNR | 21.9–25.6 | 20.1–24.8 | 22.6–26.8 | 23.0–33.7 | 21.9–33.2 | 25.6–29.7 | – |

IL, insertion loss.

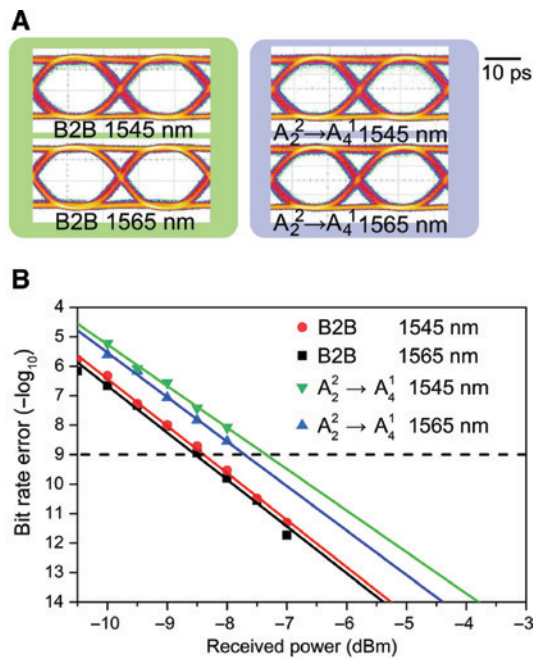


Figure 5: The power penalties for the error-free switching ($\text{BER} < 10^{-9}$) are 1.0 dB and 0.8 dB at 1545 nm and 1565 nm. (A) Eye-diagram and (B) bit-error-rate of routing path $A_2^2 \rightarrow A_4^1$ at the wavelength of 1545 nm and 1565 nm.

wavelength range of 1525–1565 nm. If each channel carries a signal with the data rate of 40 Gbps, the total throughput is 2 Tbps for each routing path.

4 Conclusion

In summary, we propose and experimentally demonstrate a five-port non-blocking optical router based on mode-selective

routing. It utilizes four spatial modes to distinguish routing paths and can passively direct specific spatial mode from the source port to the destination port intelligently without power consumptions and additional switching time. The architecture is constructed by mode-multiplexers/de-multiplexers, waveguide crossings and single-mode interconnect waveguides. The footprint of the five-port router is 1 mm × 0.5 mm. Experimental results show that the insertion loss of its 20 routing paths are less than 8.5 dB and the OSNRs are larger than 16.3 dB in the worst case. To characterize its routing functionality, a 40-Gbps data transmission is implemented. The device we present expands the library of optical router and creates possibilities for more future applications combining MDM and passive optical router.

Acknowledgments: This work was supported by the National Key R&D Program of China under grant 2017YFA0206402 and the National Natural Science Foundation of China (NSFC) under grants 61235001, 61575187, 61505198, 61535002, and 61704168.

References

- [1] Haurylau M, Chen G, Chen H, et al. On-chip optical interconnect roadmap: challenges and critical directions. *IEEE J Sel Top Quant Electron* 2006;12:1699–705.
- [2] Schares L, Kash JA, Doany FE, et al. Terabus: terabit/second-class card-level optical interconnect technologies. *IEEE J Sel Top Quant Electron* 2006;12:1032–44.
- [3] Miller DAB. Device requirements for optical interconnects to silicon chips. *Proc IEEE* 2009;97:1166–85.
- [4] Shacham A, Bergman K, Carloni LP. Photonic networks-on-chip for future generations of chip multiprocessors. *IEEE Trans Comput* 2008;57:1246–60.

- [5] Sherwood-Droz N, Wang H, Chen L, et al. Optical 4×4 hitless silicon router for optical networks-on-chip (NoC). *Opt Express* 2008;16:15915–22.
- [6] Biberman A, Lee B, Sherwood-Droz N, Lipson M, Bergman K. Broadband operation of nanophotonic router for silicon photonic networks-on-chip. *IEEE Photon Technol Lett* 2010;22:926–8.
- [7] Yang M, Green W, Assefa S, et al. Non-blocking 4×4 electro-optic silicon switch for on-chip photonic networks. *Opt Express* 2011;19:47–54.
- [8] Hu T, Qiu H, Yu P, et al. Wavelength-selective 4×4 nonblocking silicon optical router for networks-on-chip. *Opt Lett* 2011;36:4710–2.
- [9] Tan X, Yang M, Zhang L, Jiang Y, Yang J. A generic optical router design for photonic network-on-chips. *J Lightwave Technol* 2012;30:368–76.
- [10] Hu T, Shao H, Yang L, et al. Four-port silicon multi-wavelength optical router for photonic networks-on-chip. *IEEE Photon Technol Lett* 2013;25:2281–4.
- [11] Ji R, Yang L, Zhang L, et al. Five-port optical router for photonic networks-on-chip. *Opt Express* 2011;19:20258–68.
- [12] Gu H, Mo K, Xu J, Zhang W. A low-power low-cost optical router for optical networks-on-chip in multiprocessor systems-on-chip. In: *Proceedings of the IEEE Computer Society Annual Symposium on VLSI*, Tampa, FL, USA; 2009;19–24.
- [13] Xie Y, Xu J, Zhang J, Wu Z, Xia G. Crosstalk noise analysis and optimization in 5×5 hitless silicon-based optical router for optical networks-on-chip (ONoC). *J Lightwave Technol* 2012;30:198–203.
- [14] Chen L, Chen Y. Compact, low-loss and low-power 8×8 broadband silicon optical switch. *Opt Express* 2012;20:18977–85.
- [15] Fan G, Orobitchouk R, Han B, Li Y, Li H. 8×8 Wavelength router of optical network on chip. *Opt Express* 2017;25:23677–83.
- [16] Tanizawa K, Suzuki K, Toyama M, et al. Ultra-compact 32×32 strictly-non-blocking Si-wire optical switch with fan-out LGA interposer. *Opt Express* 2015;23:17599–606.
- [17] Lu L, Zhao S, Zhou L, et al. 16×16 Non-blocking silicon optical switch based on electro-optic Mach-Zehnder interferometers. *Opt Express* 2016;24:9295–307.
- [18] Luo Q, Zheng C, Huang X, Wang Y, Zhang D. Polymeric N-stage serial-cascaded four-port optical router with scalable 3N channel wavelengths for wideband signal routing application. *Opt Quant Electron* 2014;46:829–49.
- [19] Ye X, Yin Y, Yoo SB, Mejia P, Proietti R, Akella, V. DOS: a scalable optical switch for datacenters. In: *Proceedings of the 6th ACM/IEEE Symposium on Architectures for Networking and Communications Systems*, La Jolla, California, USA, 2010; 24.
- [20] Kawaguchi Y, Tsutsumi K. Mode multiplexing and demultiplexing devices using multimode interference couplers. *Electron Lett* 2002;38:1.
- [21] Greenberg M, Orenstein M. Multimode add-drop multiplexing by adiabatic linearly tapered coupling. *Opt Express* 2005;13:9781–387.
- [22] Driscoll JB, Grote RR, Souhan B, Dadap JI, Lu M, Osgood RM. Asymmetric Y junctions in silicon waveguides for on-chip mode-division multiplexing. *Opt Lett* 2013;38:1854–6.
- [23] Qiu H, Yu H, Hu T, et al. Silicon mode multi/demultiplexer based on multimode grating-assisted couplers. *Opt Express* 2013;21:17904–11.
- [24] Wang J, He S, Dai D. On-chip silicon 8-channel hybrid (de) multiplexer enabling simultaneous mode- and polarization-division-multiplexing. *Laser Photonics Rev* 2014;8:18–22.
- [25] Luo LW, Ophir N, Chen CP, et al. WDM-compatible mode-division multiplexing on a silicon chip. *Nat Commun* 2014;5:3069.
- [26] Xu H, Shi Y. Dual-mode waveguide crossing utilizing taper-assisted multimode-interference couplers. *Opt Lett* 2016;41:5381–4.
- [27] Gabrielli LH, Liu D, Johnson SG, Lipson M. On-chip transformation optics for multimode waveguide bends. *Nat Commun* 2012;3:1217.
- [28] Chen CH, Chiu CH. Taper-integrated multimode-interference based waveguide crossing design. *IEEE J Quant Electron* 2010;46:1656–61.
- [29] Fang Q, Liow T, Song J, et al. Suspended optical fiber-to-waveguide mode size converter for silicon photonics. *Opt Express* 2010;18:7763–9.
- [30] Jia L, Song J, Liow T, et al. Mode size converter between high-index-contrast waveguide and cleaved single mode fiber using SiON as intermediate material. *Opt Express* 2014;22:23652–60.